ASSESSING THE RELATIVE IMPACT OF RESUSPENDED SEDIMENT AND PHYTOPLANKTON COMMUNITY COMPOSITION ON REMOTE SENSING REFLECTANCE

Trisha Bergmann, Institute of Marine and Coastal Sciences, Rutgers University, 71 Dudley Rd, New Brunswick, NJ, 08901.
Judith Budd, Department of Geological Engineering and Sciences, Michigan Technological University, Houghton, Michigan
Gary Fahnenstiel, NOAA, Great Lakes Environmental Research Laboratory, 1431 Beach St., Muskegon, MISteven Lohrenz, University of Southern Mississippi, Department of Marine Science, MS
David Millie, Florida Marine Research Institute, FWCC & Florida Institute of Oceanography, Saint Petersburg, FLOscar Schofield, Institute of Marine and Coastal Sciences, Rutgers University, 71 Dudley Rd, New Brunswick, NJ

ABSTRACT

As part of the Coastal Ocean Processes-Episodic Events in the Great Lakes Experiment (CoOP-EEGLE) remote sensing and *in-situ* optical data was collected during an episodic turbidity plume in southern Lake Michigan in spring 1999 and 2000. The interaction of the spring bloom, riverine input, and the recurrent sediment plume provided a wide range of optical conditions to help refine coastal ocean color algorithms and served as a model testing ground for quantifying the impacts of a spectrally-restricted light field on remote sensing reflectance signals and phytoplankton communities. Measured inherent optical properties (IOPs) were used to compute spectral radiance distributions and calculate associated apparent optical properties (AOPs) using Hydrolight 4.2. Measured and modeled remote sensing reflectance (Rrs) and diffuse attenuation coefficients (Kd) showed good agreement. Onshore stations with riverine input were dominated by a high colored dissolved organic matter (CDOM) load and associated high blue absorption. Within the recurrent sediment plume absorption and scattering were both increased, but light attenuation was dominated by scattering and relative scattering/absorption ratios doubled. Offshore stations were dominated by phytoplankton absorption signatures which tended to be dominated by cryptophytes As phycobilin-containing algae became the dominant species, chlorophyll algorithms that use traditional blue/green reflectance ratios were compromised due to the high absorption of green light by phycobilin pigments. This is a notable difficulty in coastal areas, which have highly variable phytoplankton composition and are often dominated by sharp fronts of phycobilin and non-phycobilin containing algae.

INTRODUCTION

The main circulation patterns in Lake Michigan are primarily wind driven. This is an energetic and dynamic environment and it is often seriously affected by short-term episodic events. In the Great Lakes, episodic events are most frequent in the late winter/early spring when high winds and storms are prevalent and thermal stratification is low (Lee and Hawley 1998; Lou et al. 2000; Beletsky and Schwab 2001). These events

have been hypothesized to play a disproportionately large role in structuring physical and biological systems, but investigating their importance is difficult given the limitations of traditional sampling techniques.

One annual event that occurs in southern Lake Michigan each spring is a recurrent turbidity plume that extends up to 200 km alongshore (Mortimer 1988). Spring in Lake Michigan is marked by frequent, highly energetic storms, turbulent shoreline erosion, and high river runoff. These forces lead to significant resuspension of particles, which are then transported to the southern basin of the lake. The erosive forces in Lake Michigan are episodic in nature and for many biogeochemically important materials this resuspension and transport of sediments in the Southern Basin is greater than external inputs from rivers (Eadie et al. 1984; Hawley 1991; Eadie et al. 1996). Particles resuspended during the plume event may comprise up to 25% of the total transport of sediment to the southern part of the Lake (Eadie et al. 1996; Lou et al. 2000). This resuspension and transport of concentrated sediment loads is coincident with the spring phytoplankton bloom (Mortimer 1988). The spring bloom is a crucial time for the ecology of Lake Michigan as it may contribute up to 50% of the total annual primary production in the Lake and is a major source of carbon to higher trophic levels (Fahnensteil and Scavia 1987). The physical processes associated with these coastal plumes were believed to be critical in controlling biogeochemical cycling, shaping the light environment, altering available nutrient concentrations, establishing conditions for the spring bloom, and structuring biological communities (Mortimer 1988).

The recurrent turbidity event was first observed in remote sensing data as a highly reflective band nearshore (Mortimer 1988). At that time, Mortimer noted the difficulty in using optical and remote sensing techniques in areas of strong optical gradients and highly variable concentrations of suspended particulate material (SPM), colored dissolved organic matter (CDOM), and chlorophyll such as that observed in coastal areas. Since that time there has been much debate over the utility of such techniques in dynamic coastal environments. Recent efforts have focused on remote sensing techniques in order to increase sampling resolution to ecologically relevant scales for investigation into the effects of short-term episodic events. As part of the Episodic Events – Great Lakes Experiment (EEGLE), we wanted to quantify the effects of the episodic recurrent turbidity plume on optical parameters, phytoplankton dynamics, and remote sensing techniques and algorithm development.

DATA COLLECTION AND PROCESSING

Sampling was conducted in the southeastern portion of Lake Michigan (Fig. 1) from 24-26 March 1999, 14-15 and 22-24 April 1999, and 18-19 March 2000 onboard the R/V Laurentian. Sampling stations were established both inside and outside of the sediment plume along historic transect lines perpendicular to the coast. Vertical profiles of physical and optical parameters were performed at each station and supplemented with discrete water samples that were taken to the laboratory for more in depth analysis.

At each station, hydrographic profiles of the water column were measured with a SeaBird CTD. Optical measurements included surface and vertical profiles of both apparent and inherent optical properties. Inherent optical properties (IOPs) were measured with a dual-path absorption and attenuation meter (AC-9; Wetlabs Inc.). The

AC-9 measures both absorption and attenuation at 9 wavelengths of light (412, 440, 488, 510, 532, 555, 676, and 715 nm). The AC-9 was factory calibrated between sampling years and calibrated daily using ultra-clean water from a Barnstead E-Pure water purification system. Absorption data were integrated with concurrently collected CTD data and were temperature (Pegau et al. 1997) and scattering (Zaneveld and Kitchen 1994) corrected and binned to 0.25m depth intervals.

Apparent optical properties (AOPs) were collected using a profiling spectral radiometer (Ocean Color Radiometer 200; Satlantic Inc.) and a hyperspectral radiometric buoy (HTSRB; Satlantic Inc.). The OCR-200 measures downwelling irradiance (E_d) and upwelling radiance (L_u) *in-situ* as well as downwelling surface irradiance [$E_d(0^+)$] at 14 wavelengths (305, 324, 339, 380, 406, 412, 443, 490, 510, 555, 619, 665, 670, and 705 nm). The TSRB measures $E_d(0^+)$ and L_u (at 0.7m) at 123 visible wavelengths. All Satlantic sensors were factory calibrated prior to each sampling year. Collected radiometric data were processed using Satlantic's Prosoft software package according to manufacturer protocols. No dark corrections or self shading corrections were applied to these data. Diffuse attenuation coefficient (K_d) values were calculated as

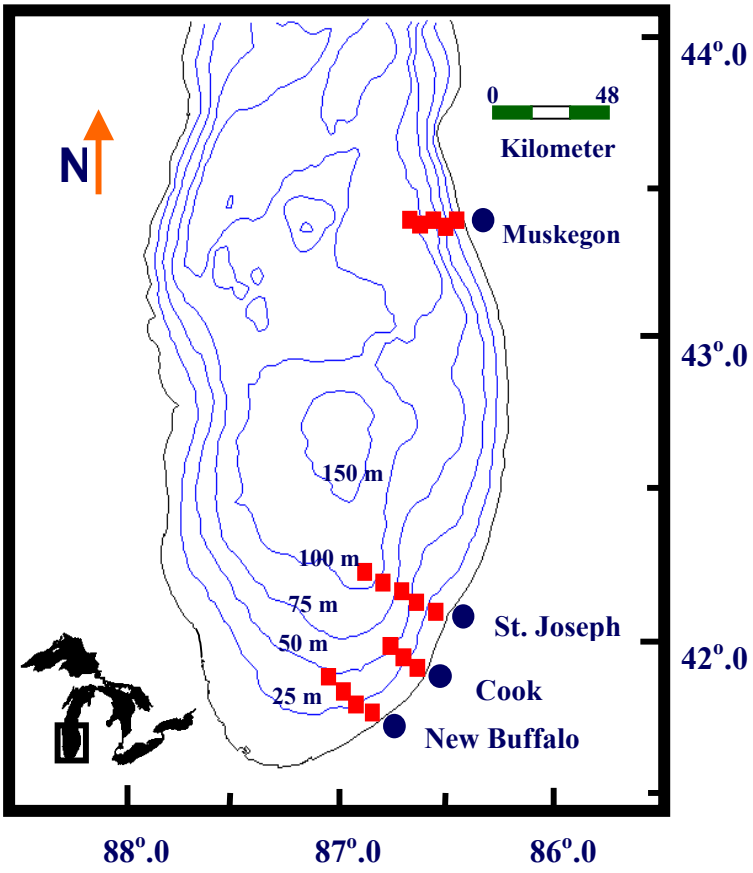

Figure 1: Sampling locations in southeastern Lake Michigan occupied in 1998 - 2000.

$$K_d = LN\left(\frac{Ed_2}{Ed_1}\right)\frac{1}{\Delta z}$$

and remote sensing reflectance (Rrs) values were calculated using Prosoft as

$$Rrs(0^+,\lambda) = \frac{L_w(0^+,\lambda)}{E_d(0^+,\lambda)}$$

where L_w is upwelling radiance propagated up through the surface of the water as

$$L_w(0^+,\lambda) = 0.54 L_w(0^-,\lambda)$$

Remote sensing reflectance outputs from Prosoft calculations were subsequently used for calculation of chlorophyll *a* concentrations using an array of remote sensing chlorophyll algorithms [Table 1 (O'Reilly et al. 1998; O'Reilly et al. 2000)].

Sensor	Equation	R
SeaWiFS/OC2	$C = 10.0^{(0.341-3.001R+2.811R^2-2.041R^3)} - 0.04$	490/555
OCTS/OC4O	$C = 10.0^{(0..405-2.900R+1.690R^2-0.530R^3-1.144R^4)}$	443>490>520/565
MODIS/OC3M	$C = 10.0^{(0.2830-2.753R+1.457R^2-0.659R^3-1.403R^4)}$	443>490/550
CZCS/OC3C	$C = 10.0^{(0.362-4.066R+5.125R^2-2.645R^3-0.597R^4)}$	443>520/550
MERIS/OC4E	$C = 10.0^{(0.368-2.814R+1.456R^2+0.768R^3-1.292R^4)}$	443>490>510/560
SeaWiFS/OC4v4	$C = 10.0^{(0.366-3.067R+1.930R^2+0.649R^3-1.532R^4)}$	443>490>510/555
SeaWiFS/OC2v4	$C = 10.0^{(0.319-2.336R+0.879R^2-0.135R^3)} - 0.071$	490/555

Table 1: Algorithms used to calculate chlorophyll a from remote sensing reflectance. R is determined as the maximum of the values shown. Sensor algorithms shown are for SeaWiFS (Sea-viewing Wide Field of view Sensor), OCTS (Ocean Color and Temperature Scanner), MODIS (Moderate Resolution Imaging Spectroradiometer, CZCS (Coastal Zone Color Scanner), and MERIS (Medium Resolution Imaging Spectrometer).

Teflon-coated Niskin bottles, lowered to selected depths, were used to collect water for assessment of phytoplankton photopigments and microphotometry assays. Phytoplankton biomass, as chlorophyll *a*, and phylogenetic group dynamics were characterized using chemotaxonomic pigments derived using High Performance Liquid Chromotography as outlined in (Millie et al. 2002, in press). Microphotometry assays were conducted as in (Bergmann et al. 2002, submitted).

In order to evaluate the dynamic response of primary producers to the highly variable *in-situ* light environment, we needed to spectrally characterize the underwater light field under a wide range of conditions. Establishing a solid relationship between the IOPs and AOPs provides confidence that a full set of radiometric parameters can be calculated given *in situ* measurements of the IOPs. A subsection of our data set (n=41 profiles) was input into Hydrolight 4.2 (Sequoia Scientific Inc.) to numerically solve the radiative transfer equation for a realistic radiance distribution. Hydrolight requires four

basic input parameters; the IOPs of the water body, wind speed, sky spectral radiance distribution, and water column bottom boundary conditions. In this study we supplied Hydrolight with measured IOPs (a and c) from an AC-9 and measured wind speeds from an anemometer aboard the research vessel. The sky spectral radiance distribution is calculated within Hydrolight via RADTRAN based upon user-supplied date, time of day, location on the globe, and cloud cover at each station. Reflectance of the bottom boundary was set at 20% without spectral dependence for all calculations. Additional inputs include chlorophyll concentrations and the backscatter fraction (bb/b). Chlorophyll concentrations were not included because measured values were not available for all calculations. The backscatter fraction was optimized at each individual station to minimize the difference between the output and measured values and input as a Fournier –Fourand (FF) phase function. In the absence of a measured particle phase function, the FF is an acceptable replacement as the exact shape of the phase function is not as critical as the magnitude of the backscatter ratio for calculations of the AOPs (Mobley et al. 2002).

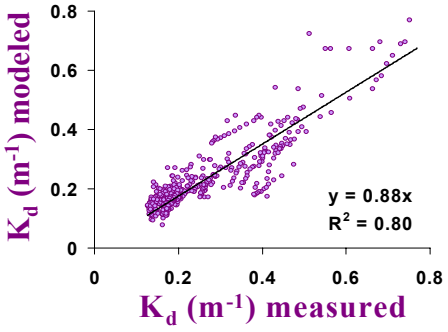

Figure 2: Modeled vs. measured diffuse attenuation coefficient (K_d) for PAR. The solid line is the best fit line with an intercept at the origin.

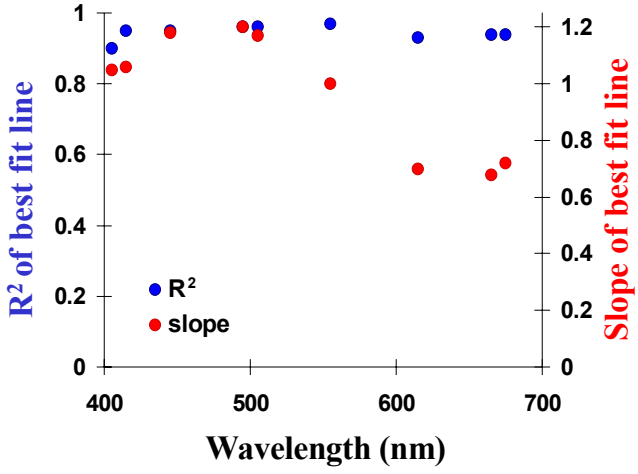

Figure 3: Modeled vs. measured remote sensing reflectance correlation results.

To validate our results from Hydrolight, modeled values were compared to concurrently measured AOPs at 41 stations in our sampling area over the course of two years in the spring and summer. These stations encompass a wide variety of optical and physical environments. To correlate K_d, we incorporated 435 data points over spatial and temporal gradients and directly compared the output with measured values (Fig. 2). The correlation was strong with a slope of 0.88 indicating that modeled values were slightly underestimating measured K_d values. Rrs correlations were also strong (average $R^2 = 0.94$) although spectrally dependent (Fig. 3). The slope was very close to 1.0 at lower wavelengths and dropped off towards the red wavelengths (slope range = 0.68 – 1.2).

Hydrolight output was used to quantify the spectral availability of light at depth. This light field is represented by the scalar irradiance (E_o). E_o is the integral of the radiance over all angles around a point. This differs from the downwelling irradiance (E_d), which is the traditionally measured irradiance term. E_d accounts only for light

propagating in the downward direction and proportionally weights the contribution of radiation at different incidence angles. The E_o output from Hydrolight calculations allowed us to use this E_o term, which we were unable to measure. E_o values were used to calculate the scalar diffuse attenuation coefficient (K_o),

$$K_o = LN\left(\frac{Eo_2}{Eo_1}\right)\frac{1}{\Delta z}$$

the scalar optical depth (ζ_o),

$$\zeta_o = K_o z$$

and the average cosine,

$$\overline{\mu} = \frac{E_d - E_u}{E_o}$$

where E_u is the upwelling irradiance.

RESULTS AND DISCUSSION

The springtime recurrent turbidity plume observed in southern Lake Michigan established a strong gradient ideal for assessing the utility of optical techniques in coastal

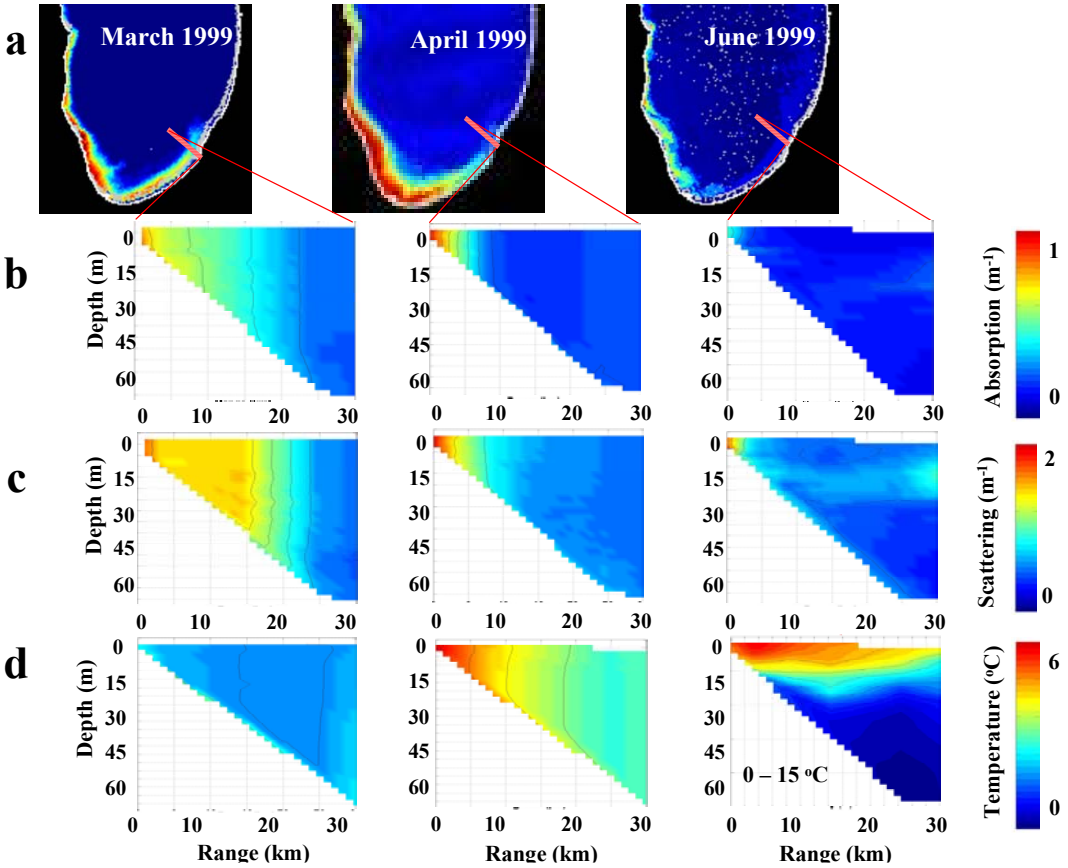

Figure 4: The temporal evolution of the southern Lake Michigan recurrent turbidity plume. a) AVHRR remote sensing reflectance, b) absorption, c) scattering, and d) temperature along the transect line shown extending 30km offshore St. Joseph, MI. Note the change in scale for the temperature plot associated with June 1999.

waters. The location and extent of the plume could be determined through both remote sensing and *in-situ* sampling techniques (Fig. 4). The plume region, delineated by high reflectance values, extended approximately 20 km offshore for much of the EEGLE study. As seen in previous years, the sediment plume began in the early spring and lasted until early summer. Although both absorption and scattering were increased within the plume, the changes in light climate were dominated by the increase in scattering. The three major optical zones along a transect line in April 1999 extending 32 km offshore St. Joseph, MI, through the sediment plume area, can readily be observed in collected data.

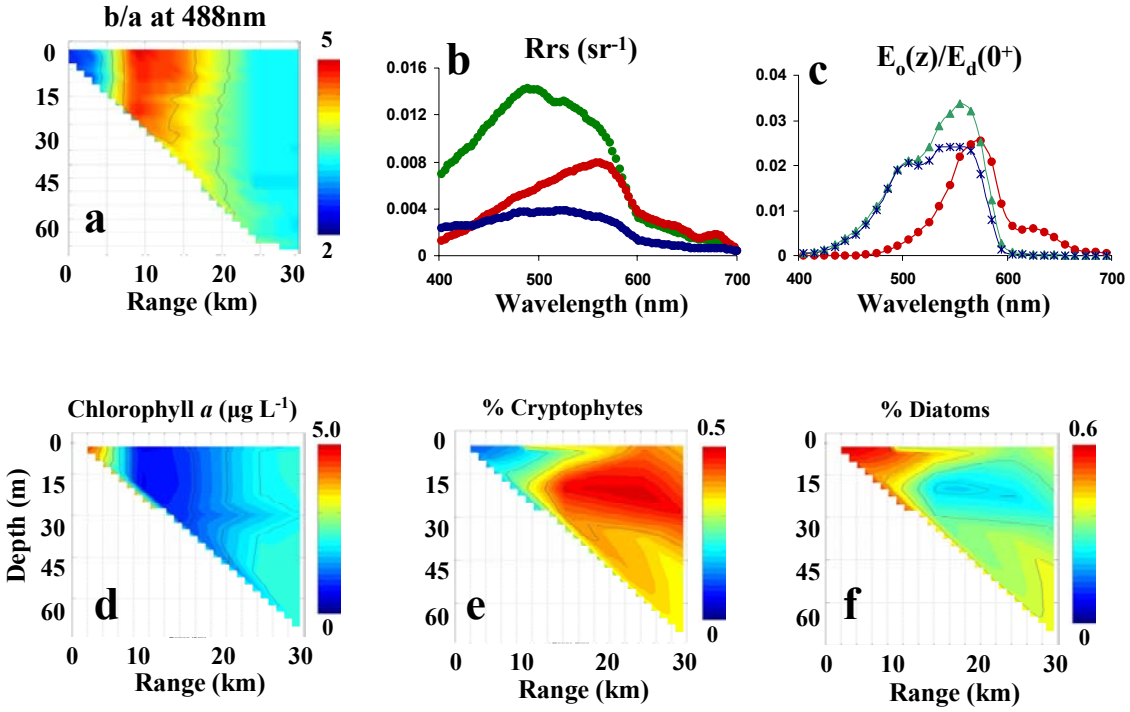

Figure 5: Optical and biological properties associated with an April 1999 cross shelf transect offshore St. Joseph, MI. a) scattering/absorption ratio at 488nm, b) remote sensing reflectance at an onshore station (red line, 2km offshore), a plume dominated station (green line, 10km offshore), and an offshore station (blue line, 30km offshore), c) fraction of available light at the 1% light level, as E_o at depth normalized to E_d at the surface (station colors as in c), d) HPLC measured chlorophyll a concentrations, e) percent of total chlorophyll a associated with cryptophytes, and f) percent of total chlorophyll a associated with diatoms.

The three distinct water types along this transect line included an onshore river/plume region that extended to roughly 10 km offshore, plume dominated water that extended approximately 10 to 20 km offshore, and offshore stations that were further than 20 km.

The sharp optical gradients encountered allowed the impact of variable in-water constituents on remote sensing reflectance to be characterized. Remote sensing reflectance at nearshore stations, affected by both the sediment plume and outflow from the St. Joseph River, showed the characteristic low blue reflectance associated with high

concentrations of CDOM and chlorophyll *a*. The St Joseph River drains a watershed area of 694,000 acres mainly through agricultural areas of Indiana and is considered a significant source of dissolved organic carbon (Mortimer 1988). Chlorophyll *a* concentrations at nearshore stations were relatively high and diatoms dominated the phytoplankton community (Fig. 5d-f). This was also apparent in the Rrs spectra as a significant decrease in the 400-500 nm region and the chlorophyll *a* fluorescence signal at 676 nm (Fig. 5b, red line). The high blue absorption at onshore stations resulted in the selective removal of blue wavelengths and a red shift of the available light field, while offshore stations had proportionally more blue and green light (Fig. 5c). Moving offshore into waters impacted less by the river, the effects of the sediment plume became more apparent. Absorption values decreased while scattering stayed high resulting in a significant increase in measured b/a ratios, which was the primary optical signature of the sediment plume (Figs. 4 and 5a). This proportional decrease in absorption and increase in scattering was reflected in higher Rrs signals due to the reflective materials in Lake Michigan which are eroded from either alongshore bluffs or shallow water glacial deposits; the sediment composition in the southeastern part of the Lake is dominated by these silts and fine sands (Scavia and Fahnensteil 1987; Eadie et al. 1996; Barbiero and Tuchman 2000). Further offshore, the optics were dominated by phytoplankton absorption. Both absorption and scattering were low relative to onshore and plume dominated waters and Rrs spectra were comparatively low and spectrally flat (Fig. 5b, blue line).

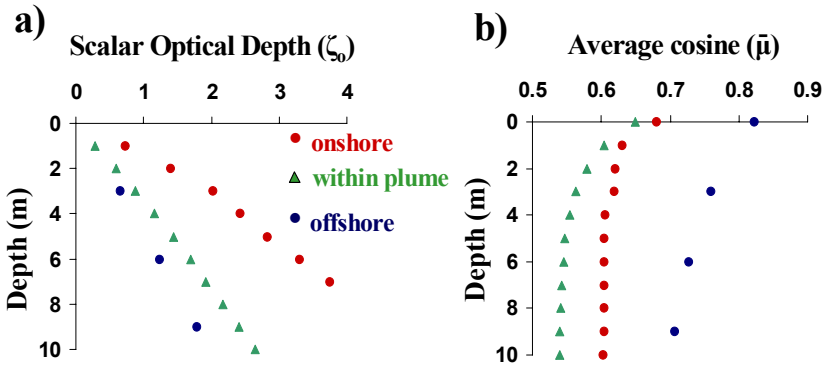

Figure 6: Vertical light properties at April 1999 stations onshore (red, 2km offshore), in plume-dominated waters (green, 10km offshore), and offshore (blue, 30km offshore) - a) scalar optical depth (ζ_o) for PAR and b) average cosine (μ) at depth for PAR.

The changes in the concentrations of optically active constituents altered the light climate of the different water types. In addition to these spectral changes in light quality, the quantity of available light at depth was decreased in onshore stations. The relationship between scalar optical depth and physical depth was steeper than in plume-dominated and offshore stations (Fig. 6a). A deeper optical depth corresponding to the same physical depth indicates that onshore waters were more attenuating than offshore waters. Although total light attenuation was also higher in plume dominated stations as compared to offshore waters, absorption was much lower and scattering was still relatively high resulting in a change in the diffusivity of the underwater light. The average cosine provides a simple description of the angular radiance distribution of the underwater light field. Average cosine values range from 0 for isotropic light fields to 1

in a collimated beam of light; a lower average cosine value indicates a more diffuse light field. In regions affected by the turbidity plume, the increased scattering resulted in a lower average cosine (Fig. 6b). The average cosine was lowest in areas most optically impacted by the plume.

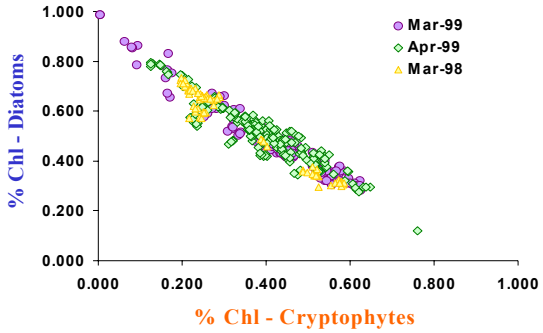

Figure 7: Percentage of total chlorophyll a associated with cryptophytes vs. percentage of total chlorophyll a associated with diatoms from CHEMTAX output for all available data.

The distribution of total chlorophyll and the composition of phytoplankton communities also varied as the optical environment changed. Diatoms consistently comprised a higher proportion of chlorophyll *a* onshore and in surface waters, while cryptophytes comprised a higher proportion offshore and deeper waters (Fig. 5d-e). This resulted in a strong inverse relationship between diatom and cryptophyte abundances (Fig. 7). The primary photosynthetic pigments for diatoms are chlorophyll and fucoxanthin, which absorb maximally in the blue and red wavelengths of light while the cryptophytes utilize phycobilin pigments, which have an absorption maximum in the green wavelengths. Although the absorption efficiencies (Qa) measured by microphotometry on a single cell for a representative diatom (*Melosira islandica*) and cryptophyte (*Rhodomonas lens*) were equal when integrated over PAR for "white" surface irradiance, they were distinctly spectrally different (Fig. 8a). Assuming that the isothermal water columns were completely vertically mixed during the spring months (Fig. 3d), an average light field was computed based upon the spectral light field within the mixed layer depth. The average light field experienced by these vertically mixed

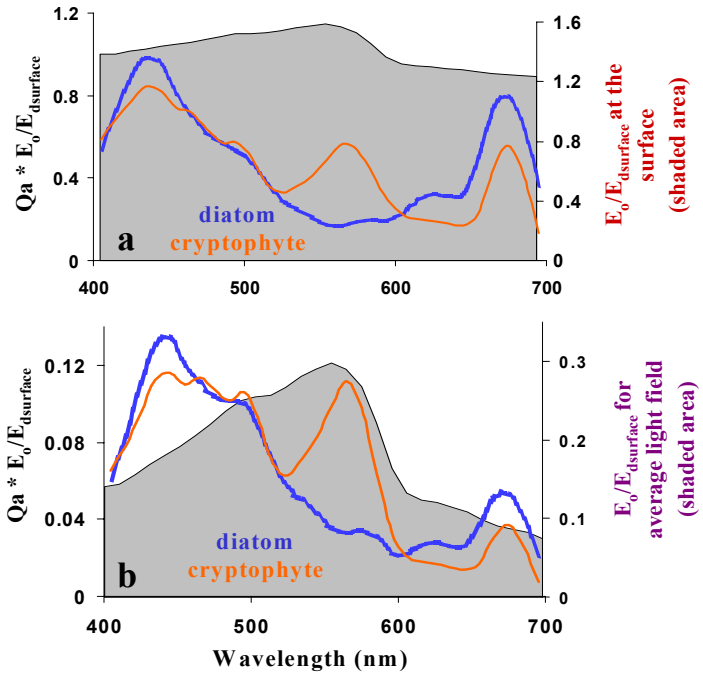

Figure 8: Product of the absorption efficiency (Qa) for a representative diatom and cryptophyte and the scalar irradiance, normalized to the downwelling irradiance, a) at the surface and b) for the average light field experienced by a phytoplankton cell over the mixed layer depth assuming total mixing of the water column.

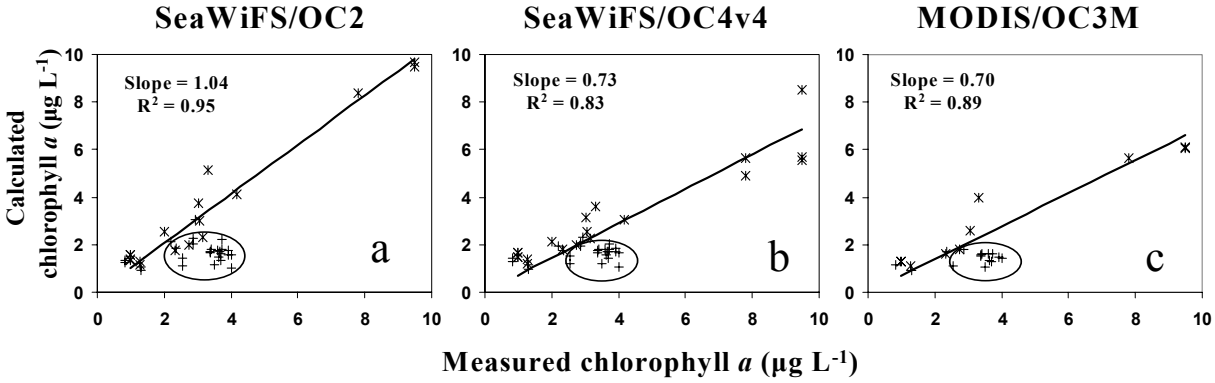

Figure 9: Relationship between measured chlorophyll a (HPLC) and calculated chlorophyll a from three currently used ocean color algorithms - a) SeaWiFS OC2, b) SeaWiFS OC4v4, and c) MODIS OC3M. The relationship is strong until the optical signal is affected by cryptophyte absorption. The circled stations are those where cryptophytes make up 40% or more of the total phytoplankton population. The solid line is the best fit line through data not including cryptophyte dominated stations; reported slope and R^2 values are for this best fit line (see Table 2).

populations in offshore stations was spectrally restricted to predominately green light. Therefore, the potential absorption was higher for cryptophytes than diatoms at depth (Fig. 8b). This spectral selection for cryptophytes may explain the offshore distribution observed in phytoplankton populations.

These observed shifts in phytoplankton community composition impacted remote sensing reflectance and thus ocean color algorithms. There was a strong correlation between measured and calculated chlorophyll concentration at most stations. However, the absorption of green light by cryptophytes selectively removes green light from the light field. Chlorophyll algorithms utilize Rrs ratios, which include 550, 555, 560, and 565 nm reflectance. These ratios assume case 1 waters where the *in-situ* absorption and

sensor/ algorithm	R	slope-all stations	R^2-all stations	slope-cryptophyte dominated stations	R^2-cryptophyte dominated stations
SeaWiFS/OC2	490/555	0.81	0.66	1.04	0.95
OCTS/OC4O	443>490>520/565	0.54	0.81	0.6	0.89
MODIS/OC3M	443>490/550	0.6	0.77	0.7	0.89
CZCS/OC3C	443>520/550	0.57	0.76	0.65	0.88
MERIS/OC4E	443>490>510/560	0.59	0.79	0.62	0.87
SeaWiFS/OC4v4	443>490>510/555	0.65	0.68	0.73	0.83
SeaWiFS/OC2v4	490/555	0.68	0.69	0.78	0.83

Table 2: Correlation results for the calculation of chlorophyll from remote sensing reflectance measurements. The slope and R^2 for the correlation between measured and calculated chlorophyll is shown (as in Fig. 12) for all stations and for a subset of stations where the phytoplankton community composition is not dominated by cryptophytes. All of the algorithms perform better in areas that were not significantly influenced by cryptophyte absorption.

water leaving radiance (L_w) signal in the blue wavelengths is dominated by chlorophyll absorption while L_w in the green will be insensitive to chlorophyll concentrations (Gordon and Morel 1983). However, in Lake Michigan, cryptophyte absorption selectively removed green light from the reflectance signal. Areas not significantly impacted by cryptophytes (less than 40% of total chlorophyll) had good agreement between measured and satellite estimated chlorophyll (Fig. 9 and Table 2). In regions with high concentrations of phycobilin containing algae, remotely estimated chlorophyll concentrations were underestimated by an average of 45% for all algorithms tested. The sediment plume had little affect on the utility of ocean color remote sensing efforts. The critical parameter impacting the performance of ocean color algorithms was the community composition of phytoplankton.

REFERENCES

Barbiero, R. and M. Tuchman (2000). Results from the Great Lakes National Program Office's Biological Open Water Surveillance Program of the Laurentian Great Lakes for 1998. Chicago, IL, US EPA Great Lakes Program.

Beletsky, D. and D. Schwab (2001). Modeling circulation and thermal structure in Lake Michigan: Annual cycle and interannual variability. JGR 106(C9): 19745-19771.

Bergmann, T., G. Fahnenstiel, S. Lohrenz, D. Millie and O. Schofield (2002, submitted). The Impacts of a Recurrent Resuspension Event and Variable Phytoplankton Community Composition on Remote Sensing Reflectance. J. Geophys. Res.

Eadie, B., R. Chambers, W. Gardner and G. Bell (1984). Sediment trap studies in Lake Michigan: Resuspension and chemical fluxes in the southern basin. J. Great Lakes Res. 10(3): 307-321.

Eadie, B., D. Schwab, R. Assel, N. Hawley, N. Lansing, G. Miller, N. Morehead, J. Robbins, P. Van Hoof, G. Leshkevich, T. Johengen, P. Lavrentyev and R. Holland (1996). Development of recurrent coastal plume in Lake Michigan observed for first time. EOS 77(35): 337-338.

Fahnensteil, G. and D. Scavia (1987). Dynamics of Lake Michigan phytoplankton: The Deep Chlorophyll Layer. J. Great Lakes Res. 13(3): 285-295.

Gordon, H. and A. Morel (1983). Remote assessment of ocean color for interpretation of satellite visible imagery. New York, Spriner-Verlag.

Hawley, N. (1991). Preliminary observations of sediment erosion from a bottom resting flume. J. Great Lakes Res. 17(3): 361-367.

Lee, C. and N. Hawley (1998). The resonse of suspended particulate material to upwelling and downwelling events in southern Lake Michigan. J. Sed. Res. 68(5): 819-831.

Lou, J., D. Schwab, D. Beletsky and N. Hawley (2000). A model of sediment resuspension and transport dynamics in southern Lake Michigan. JGR 105(C3): 6591-6610.

Millie, D., G. Fahnensteil, H. Carrick, S. Lohrenz and O. Schofield (2002, in press). Phytoplankton pigments in coastal Lake Michigan: distributions during the spring isothermal period and relation with episodic sediment resuspension. J . Phyc. 38.

Mobley, C., L. Sundman and E. Boss (2002). Phase function effects on oceanic light fields. Applied Optics 41(6): 1035-1050.

Mortimer, C. (1988). Discoveries and testable hypotheses arrising from Coastal Zone Color Scanner imagery of southern Lake Michigan. Limnol. Oceanogr. 33(2): 203-226.

O'Reilly, J., S. Maritorena, B. Mitchell, D. Siegel, K. Carder, S. Garver, M. Kahru and C. McClain (1998). Ocean color algorithms for SeaWiFS. JGR 103(C11): 24937-24953.

O'Reilly, J., S. Maritorena, M. O'Brien, D. Siegel, D. Toole, D. Menzies, R. Smith, J. Mueller, B. Mitchell, M. Kahru, F. CHavez, P. Strutton, G. Cota, S. Hooker, C. McClain, K. Carder, F. Müller-Karger, L. Harding, A. Magnuson, D. Phinney, G. Moore, J. Aiken, K. Arrigo, R. Letelier and M. Culver (2000). SeaWiFS postlaunch technical report series, Volume 11, SeaWiFS postlaunch calibration and validation analyses, Part 3, NASA Technical Memorandum.

Pegau, W., D. Gray and J. Zaneveld (1997). Absorption and attenuation of visible and near-infrared light in water: dependence on temperature and salinity. Applied Optics 36(24): 6035-6046.

Scavia, D. and G. Fahnensteil (1987). Dynamics of Lake Michigan phytoplankton: mechanisms controlling epilimnetic communities. J. Great Lakes Res. 13(2): 103-120.

Zaneveld, J. and J. Kitchen (1994). The scattering error correction of reflecting tube absorption meters. SPIE 2258: 44-55.